1997-09-01

Azimuthal Modulation of C-Band Scatterometer Over Southern Ocean Sea Ice

David G. Long
david_long@byu.edu

David S. Early

Original Publication Citation

Early, D. S., and D. G. Long. "Azimuthal Modulation of C-Band Scatterometer ÏƒÌ Over Southern Ocean Sea Ice." Geoscience and Remote Sensing, IEEE Transactions on 35.5 (1997): 121-9

Azimuthal Modulation of C-Band Scatterometer σ^o Over Southern Ocean Sea Ice

David S. Early, *Student Member, IEEE,* and David G. Long, *Member, IEEE*

***Abstract*— In a continuing evaluation of the ERS-1 C-band scatterometer as a tool for studying polar sea ice, we evaluate the azimuthal modulation characteristics of Antarctic sea ice. ERS-1 AMI scatterometer mode data sets from several study regions dispersed in the Antarctic seasonal sea ice pack are evaluated for azimuthal modulation. When appropriate, the incidence angle dependence is estimated and removed in a study region before determining whether azimuthal modulation is present in the data. Other comparisons are made using the fore and aft beam measurement difference. Our results show that over the ice pack, azimuthal modulation is less than 1 dB at the scale of observation of the ERS-1 C-band scatterometer.**

I. Introduction

SPACEBORNE scatterometers are currently used to monitor and study near-surface ocean winds on a global scale. The temporal and spatial resolution of the spaceborne scatterometer make it a useful instrument for studying these atmospheric processes. The scatterometer has also been used to study nonocean surface conditions (e.g., [1]–[5]). However, while the temporal coverage of the scatterometer is good for rapid repeat coverage of the earth's surface, the nominal spatial resolution of 25–50 km may be too coarse for detailed classification of nonocean surface conditions in some studies.

In order to improve the resolution of the scatterometer data, a resolution-enhancement technique has been developed to exploit the frequent, overlapping coverage of the spaceborne scatterometer [6]. The algorithm was originally developed for studies of the Amazon, where azimuthal modulation is assumed negligible [1]. The algorithm has subsequently been applied successfully to the Greenland ice sheet [2]. Azimuthal modulation of σ^o over sea ice could, if present, introduce errors in the enhanced-resolution imagery.

In this paper, we study azimuthal modulation of the C-band microwave signature of Southern Hemisphere sea ice and compare this with azimuthal modulation in the microwave signature of the Antarctic ice sheet in ERS-1 C-band scatterometer data. Azimuthal modulation has previously been observed over the Antarctic ice sheet using the SEASAT Ku-band scatterometer and is generated by wind induced ripples on the ice sheet surface [7]. However, given the dynamic nature of the Antarctic sea ice pack, we do not expect significant azimuth modulation over Antarctic sea ice at the scale of a spaceborne scatterometer. Such an assumption is consistent with previous observations of little or no azimuthal modulation in airborne SAR and scatterometer data from Arctic sea ice in the Labrador Sea [8].

The data used in this study is obtained by the ERS-1 active microwave instrument (AMI) scatterometer, a fan-beam scatterometer with three beams on the right side of the spacecraft with a nominal resolution of 50 km. The fore and aft beams are oriented to give identical incidence angles but azimuth angles 90° apart for corresponding measurement cells [9]. Originally designed as an instrument to measure near surface wind speeds over the ocean, the mid beam provides a measurement with a third azimuth angle to help discriminate wind speed and direction.

II. Southern Ocean Ice Characteristics

In order to understand the azimuthal modulation of σ^o over Antarctic sea ice at large scale (50 km), we require an understanding of the general surface characteristics of sea ice in that region. Although the volume of *in situ* and radar measurements in the Antarctic is much smaller than similar Arctic measurements, there is sufficient data to make a large scale characterization of Antarctic sea ice [4], [10].

A. Surface Characteristics

In general, the Antarctic ice pack can be divided into two regimes—an outer ice pack and an inner ice pack—and for this study, we use the definitions of these regimes as presented in [11]. Each regime has distinct physical properties that modulate microwave signatures of the ice as described below. The outer ice regime has two distinct phases: one during the winter freeze up and another during the summer melt.

The outer ice regime consists of the Marginal Ice Zone (MIZ), which is the extreme edge of the sea ice pack with a seasonally dependent makeup consisting of sea ice floes (up to several meters) surrounded by open water or slush [11]. The first phase of the outer ice regime occurs during early winter through early spring, when thermodynamic growth causes a rapid advance of the sea ice pack. The outer ice pack, and particularly the MIZ, are, by definition, regions of unsolidified or uncoalesced ice during winter freeze up; therefore, wave action in this region makes pancake ice predominant in early winter [12], [13]. A photograph of pancake ice taken at the edge of the ice pack is shown in Fig. 1 and illustrates the development of pancake ice in the outer ice regime. Oscillatory wave action pushes grease ice, new ice, and slush together, and eventually, thermodynamic cooling causes the pancakes to solidify. Before pancake ice fields coalesce, the spaces

Manuscript received April 9, 1996; revised January 9, 1997. This work was supported in part by a NASA Global Change Research Fellowship and in part by the NASA Polar Research Program under Dr. R. Thomas.

The authors are with Brigham Young University, Provo, UT 84601 USA (e-mail: earlyd@newt.ee.byu.edu; long@ee.byu.edu).

Publisher Item Identifier S 0196-2892(97)04112-0.

Fig. 1. Photograph of pancake ice taken near the Antarctic ice pack edge. Note the edges on the pancakes that are formed by wind and wave action forcing pancakes together and piling up the edge. (Courtesy of Dr. Mark Drinkwater, JPL).

surrounding the pancakes are either open water, frazil, or grease ice. Thermodynamic effects will eventually cause the pancake field to coalesce into a solid ice pack. The second phase of the outer ice zone occurs during the spring and summer melt and break up of the sea ice pack. With the spring and summer warming, the pack ice begins to break up and melt, resulting in the MIZ containing large volumes of small, broken floes and brash ice.

The inner ice pack is typically thin to thick first-year ice. Evidence from passive microwave systems shows that multiyear ice can survive in the Antarctic, and it tends to be concentrated in the western Weddell Sea along the eastern edge of the Antarctic Peninsula [14]. Ridging, which is a major contributor to large-scale deformation in Arctic sea ice, is in general much less intense in the Antarctic than in the Arctic with a lower average ridge height and lower frequency in the main body of the sea ice pack [15], [16]. In addition, as the ice ages, floes in the pack can be laden with snow to cause a negative freeboard condition, flooding the snow-ice interface. The existence of this wet slush layer changes the microwave properties of the sea ice, as does the subsequent refreezing of this slush layer [4].

B. Azimuthal Modulation in the Antarctic

Azimuthal modulation of σ^o has been observed over the Antarctic ice sheet. Using Ku-Band SEASAT scatterometer data, Remy *et al*. [7] demonstrated that observed azimuthal modulation over the Antarctic ice sheet is related to the katabatic winds on the continent. Further, any oriented scatterers, including sastrugi, wind-oriented drifts, and crevasse fields, may create azimuthal modulation in the satellite data. Ice sheets, even without significant oriented scatterers on the surface, can create azimuth modulation if there is a significant surface slope (e.g., a glacier in a mountain valley).

Sea ice, on the other hand, has surface characteristics that are very different from land ice sheets. Small-scale waves such as millimeter, capillary, or gravity waves are absent in the outer ice regime and the rest of the sea ice pack because of the presence on the ocean surface of either solidified pack ice, pancake ice in its various forms, or grease ice, which prevent the formation of these small scale waves, eliminating one source of oriented scatterers in the ice pack. Additionally, the presence of water in the upper snow layer in some areas of the sea ice pack will change the structure of wind-etched surface features such as sastrugi. To further reduce the effects of any oriented scatterers that do develop on the sea ice surface, the dynamic motion of the ice surface causes a randomization of the scatterers over a large scale, reducing the cumulative effect of scatterers on the return signal.

Since the sea ice floats on the surface of the ocean, we expect no inherent large-scale surface slope associated with sea ice that would induce azimuthal modulation. However, because the ice in the outer ice regime is defined as uncoalesced ice, long wavelength swell waves are capable of traveling through these outer regions of the sea ice pack [17] and inducing some surface slope. In the Southern Ocean, long wavelength swell waves, with wavelengths of several hundred meters and amplitudes of up to several meters, are capable of traveling hundreds of kilometers into the sea ice pack through pancake ice regions [22]. Once the pancakes have begun to coalesce and solidify, however, the waves are quickly damped out by the increasingly rigid sea ice pack.

In the absence of significant wave action, any slope in the sea ice must result from ridging or stacking of ice floes. However, the divergent nature of the sea ice pack causes break up, rotation, and refreezing of sections of the ice that effectively randomizes small-scale ridges, and other oriented scatterers may form on the surface of the sea ice. This study concentrates on microwave scattering characteristics of Antarctic sea ice on the scale of the ERS-1 AMI scatterometer (50 km), and we postulate that over the majority of the sea ice pack, relatively small structure variations in the sea ice surface will not introduce substantial azimuthal variation in the scatterometer data due to the randomizing effects of the sea ice pack motion. We shall also establish that long-wavelength swell wave penetration in the MIZ will not introduce substantial azimuthal modulation in the scatterometer signature.

III. Procedures

Sea ice surface characteristics have significant spatial and temporal variation over a basin-wide area [3]. As a result, small study regions are used. Additionally, there is a dependence of σ^o on incidence angle that must be accounted for.

Further, correlation between azimuth and incidence angles for a given cell resulting from the orbit geometry can bias azimuthal modulation evaluation. In the following section, σ^o dependence on incidence angle is discussed, and a method for removing the dependence based on a linear model is presented. This is followed by a discussion of study region selection methodology that addresses the issues of spatial and temporal variation of the surface.

A. Removal of Incidence Angle Dependence

Since the radar return may have both incidence and azimuth angle dependence, the separation of any incidence angle dependence from the data is crucial for proper interpretation of any azimuthal modulation observed in the plots. Data collected over several days may have many different incidence angles, and direct comparison of all measurements in a data set necessitates the removal of incidence angle dependence for some analyses.

To aid in this removal, we use a very simple model. Over a limited incidence angle range of 25–55°, the incidence angle dependence of the ERS-1 C-band scatterometer backscatter is approximately linear in decibels. Although the actual incidence angle dependence of σ^o in decibels is nonlinear, the linear model works very well for the midrange incidence angles, as observed in the actual and theoretical backscatter results illustrated in [8], [18], and [19]. The linear model is given by

$$\sigma^o_{\mathrm{dB}} = \mathcal{A} + \mathcal{B}(\theta - 40^\circ) \tag{1}$$

where σ^o_{dB} is the received backscatter in decibels, and θ is the incidence angle of the measurement. Although 40° is used here, the data can be normalized to any incidence angle value. $\mathcal{B}$ represents the slope of the data with respect to the incidence angle θ. An estimate of the parameter $\mathcal{B}$, which is denoted $\widehat{\mathcal{B}}$, is determined from a linear regression of the σ^o measurements for each study region. With a $\widehat{\mathcal{B}}$ estimated for a given study region, the estimate $\widehat{\mathcal{A}}_i$ for each backscatter measurement σ^o_i in the study region is given by

$$\widehat{\mathcal{A}}_i = \sigma^o_i - \widehat{\mathcal{B}}(\theta_i - 40^\circ). \tag{2}$$

The resulting $\widehat{\mathcal{A}}_i$ values represent incidence angle normalized backscatter values, i.e., the value of σ^o_i at $\theta = 40^\circ$.

B. $\widehat{\mathcal{B}}$ Error

Note that each σ^o measurement in a study region data set represents a unique backscatter measurement from a single radar footprint. The surface area of the footprint is smaller than the total area in each study region; therefore, it is reasonable to assume that due to spatial variability within the study region, each σ^o measurement may have a unique $\mathcal{B}$ associated with it. Error is introduced by using a single estimate of the $\mathcal{B}$ parameter to determine all of the incidence angle normalized backscatter estimates $\mathcal{A}_i$ in a given study region, and although the linear model in (1) is a good approximation of the incidence angle dependence, some error is realized from using the linear model.

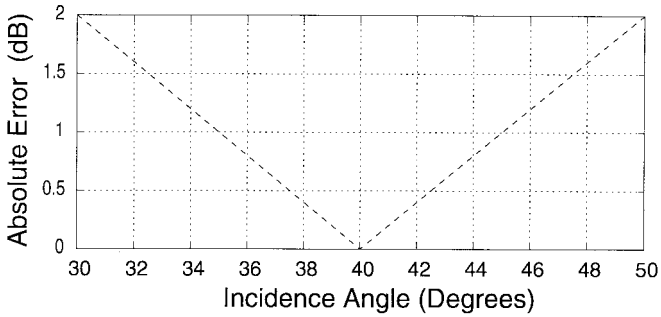

Fig. 2. Plot of the maximum error in $\widehat{\mathcal{A}}$ caused by a worst-case $\widehat{\mathcal{B}}$ error. This graph shows an example where the measurements are normalized to 40°. Note that the error for the worst case is less than 0.5 dB for an incidence angle range of ±2° around the normalization angle. It is expected that the error will be considerably less in practice than the worst-case error.

Suppose that for a given measurement σ^o_i, the true value of $\mathcal{A}$, $\mathcal{A}_t$ is given by

$$\mathcal{A}_t = \sigma^o_i - \mathcal{B}_t(\theta_i - 40^\circ) \tag{3}$$

where $\mathcal{B}_t$ represents the true $\mathcal{B}$ value for the ith measurement σ^o_i. If $\widehat{\mathcal{B}}$ is not exactly equal to the true value $\mathcal{B}_t$, the error in the estimate $\widehat{\mathcal{A}}_i$ is given by

$$\begin{aligned}\Delta\mathcal{A} &= \mathcal{A}_t - \widehat{\mathcal{A}}_i \\ &= (\widehat{\mathcal{B}} - \mathcal{B}_t)(\theta_i - 40^\circ).\end{aligned} \tag{4}$$

Introducing similar notation for the error in $\widehat{\mathcal{B}}_i$, let $\Delta\mathcal{B} = \widehat{\mathcal{B}}_i - \mathcal{B}_t$. If we assume that $\Delta\mathcal{B}$ is bounded by some maximum value, the maximum error in $\widehat{\mathcal{A}}_i$ becomes

$$\Delta\mathcal{A}_{\max} = \pm\Delta\mathcal{B}_{\max}(\theta - 40^\circ). \tag{5}$$

For the purposes of evaluating error, we can assume, based on the average $\mathcal{B}$ in Tables I and II for the regions evaluated in this study, that the mean $\mathcal{B}$ is approximately -0.2 with a worst-case range of 0.0 to -0.4, making $\Delta\mathcal{B}_{\max} = \pm 0.2$. $\Delta\mathcal{A}_{\max}$ is plotted versus incidence angle in Fig. 2.

Because the data can be normalized to any angle, the error introduced by removing incidence angle dependence can be minimized by normalizing the data to an angle in the middle of the incidence range of the data. Note that the graph in Fig. 2 shows the worst-case error for the assumptions in the previous paragraph; in practice, the error will be much smaller. We conclude that the error introduced by faulty $\mathcal{B}$ estimates is negligible when a small range of incidence angles is used and the normalization angle is in the middle of the incidence angle range of the data. Assuming a narrow incidence angle range (less than 6°), the error will not adversely affect evaluation of azimuthal modulation of 1 dB or more.

C. Study Region Selection

As part of an evaluation of basin-wide characteristics, study regions in several areas of the Antarctic sea ice pack are used. Relatively small study regions and short study intervals are used so that areas of relatively constant temporal and spatial variation can be studied. Selecting areas that are spatially and temporally homogeneous avoids creating study

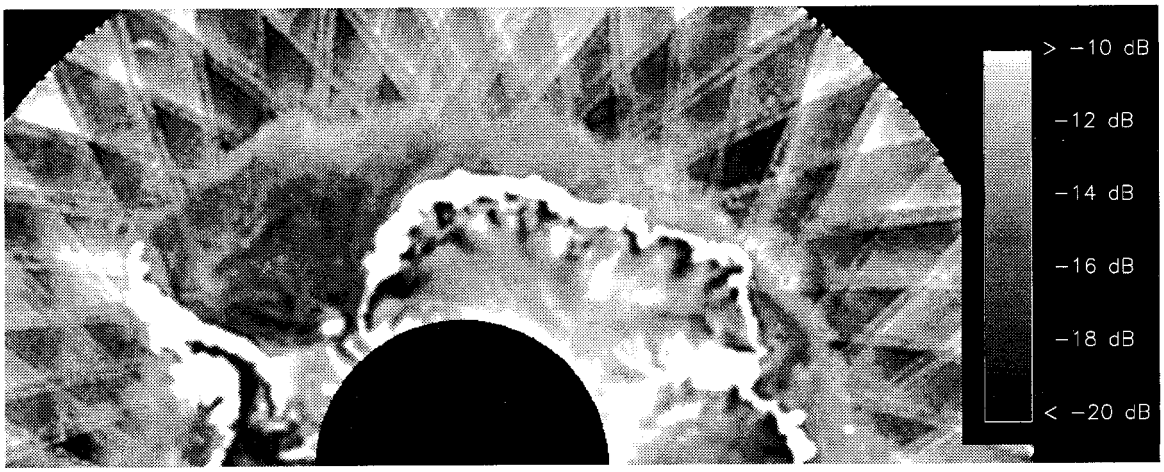

Fig. 3. Polar stereographic projection image of Antarctica. The image is generated from six days of ERS-1 data from JD 126 to JD 131, 1993. The hash marks in the periphery of the image are a result of the rapidly changing azimuthal response of the open ocean surface.

TABLE I
STUDY REGION LOCATIONS AND STATISTICS

Reg	lon x lat	1993 JD	$\hat{A}$	$\hat{B}$	σ^o Std Dev
I1	8° x 4°	23- 56	-14.41	-0.231	2.69
I2	10° x 4°	119-140	-14.68	-0.199	2.10
I3	14° x 3°	215-242	-14.85	-0.193	3.25
I5	8° x 4°	218-239	-17.26	-0.218	2.28
I6	8° x 3°	248-290	-14.63	-0.230	2.61
I7	18° x 5°	326-350	-15.14	-0.254	2.84
I8	10° x 4°	311-332	-16.80	-0.235	2.42
I10	8° x 3°	200-225	-16.56	-0.201	2.14
I11	8° x 3°	200-225	-16.05	-0.205	2.46
I12	8° x 3°	200-225	-15.81	-0.208	2.43
I13	8° x 3°	200-225	-16.44	-0.218	2.36
I14	8° x 3°	200-225	-16.33	-0.225	2.48
I15	8° x 3°	200-225	-15.65	-0.223	2.88
I16	8° x 3°	200-225	-16.94	-0.208	2.11
I17	8° x 3°	200-225	-17.12	-0.213	2.21
I18	8° x 3°	200-225	-16.92	-0.211	2.24
I19	8° x 3°	200-225	-16.86	-0.210	2.15
I20	8° x 3°	200-225	-16.80	-0.213	2.13
I21	8° x 3°	200-225	-16.60	-0.219	2.25
G1	10° x 2°	109-227	-8.07	-0.174	2.13
G2	10° x 2°	80-117	-15.42	-0.232	3.62
G3	10° x 2°	109-227	-10.56	-0.209	3.09
G4	10° x 2°	80-117	-11.59	-0.188	2.04
G5	10° x 2°	109-227	-15.01	-0.174	4.49

TABLE II
MARGINAL ICE ZONE STUDY REGION LOCATIONS AND STATISTICS

Reg	lon x lat	1993 JD	$\hat{A}$	$\hat{B}$	σ^o StdDev
M1	6° x 2°	102-120	-12.68	-0.197	2.15
M2	10° x 2°	102-120	-12.77	-0.221	2.57
M3	10° x 2°	105-120	-12.66	-0.191	2.07
M4	8° x 2°	128-146	-12.79	-0.211	2.44
M5	6° x 2°	128-146	-12.32	-0.400	5.10
M6	10° x 2°	141-161	-12.42	-0.169	1.96
M7	10° x 2°	142-161	-13.51	-0.207	2.53
M8	10° x 2°	141-161	-15.84	-0.217	2.29
M9	10° x 2°	144-164	-13.16	-0.340	4.29
M10	10° x 2°	150-170	-12.17	-0.179	2.00
M11	10° x 2°	153-173	-13.04	-0.204	2.20
M12	6° x 2°	165-181	-12.67	-0.183	2.06
M13	10° x 2°	165-181	-13.32	-0.217	2.42
M14	10° x 2°	174-181	-12.48	-0.194	2.04

regions with many different ice surfaces that might skew any azimuthal modulation evaluation. Study regions from several areas in the Southern Ocean are used to evaluate azimuthal modulation over many different sea ice surfaces. The scatterometer requires three to five days to collect enough readings for each study region to have good azimuth angle diversity. The surface conditions in each study region must be assumed constant over the data collection interval.

Study regions are chosen such that the regions are homogeneous in time and space over the data collection interval. To aid in the selection of homogeneous regions, we use a time series of enhanced-resolution images of Antarctic land and sea ice [3] to identify the largest possible regions where the spatial surface response is visually homogeneous. The spatial homogeneity of the σ^o measurements in a study region reduces the variance of the measurements, ensuring accurate assessment of low-level (<1 dB) azimuthal modulation for a given sea ice surface. Study regions that represent several different types of sea ice are selected in order to evaluate azimuthal modulation over different sea ice surfaces. An example of an enhanced-resolution Antarctic image is shown in Fig. 3. An explanation of the SIRF algorithm for generating the enhanced-resolution images is found in [20].

An additional criterion for selecting viable study regions is adequate diversity of azimuth angles. Azimuth angle diversity is required in order to properly evaluate azimuthal modulation, and this diversity is affected by the location and size of a study region and the number of days in the study interval. The scatterometer requires several days of data to generate data with good azimuthal angle diversity. If too many days of data are included, the dynamic nature of the Antarctic sea ice increases the probability that the surface will change within the study interval. However, if too few days of data are used, there will not be enough measurements to yield sufficient azimuthal diversity for modulation assessment or sufficient incidence angles to properly estimate the incidence angle dependence of the data in the study region.

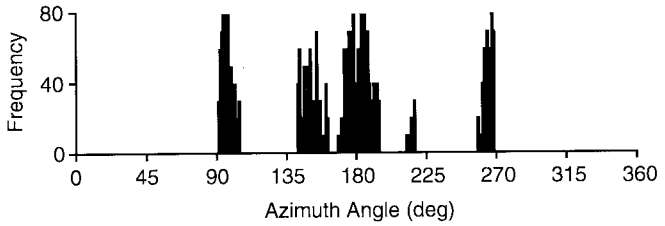

Fig. 4. Example histogram of azimuthal angles over Antarctic sea ice (Study Region I10). Note that the gaps are caused by the instrument geometry.

The successful tradeoff between study region size (spatial homogeneity) and the number of days (temporal homogeneity) in the data set is evaluated by manually examining data in each study region. An evaluation of each study region is made to determine whether the data is spatially and temporally homogeneous and whether it has sufficient azimuth angle diversity to show azimuthal modulation. The evaluation for homogeneity is done by plotting the σ^o values versus incidence angle and evaluating the data visually for σ^o spread and variance in the σ^o versus incidence angle plot, plotting the evolution of the σ^o values versus time (to evaluate temporal stability), and examining the statistics of the data. The data statistics are illustrated in Tables I and II.

To evaluate the data for azimuth angle diversity, a histogram of azimuth angles for several incidence angle ranges is plotted. An example azimuth angle histogram of ERS-1 scatterometer data over Antarctic sea ice is given in Fig. 4 for the incidence angle range 40–45°. The ERS-1 data over sea ice shows a limited range of azimuth angles. Notice the groupings of azimuth angles in the example histogram in Fig. 4. These groupings are evident in all the data used in this study and are a consequence of the ERS-1 instrument geometry and orbit. In addition, ERS-1 instrument geometry and orbit provide very few readings at azimuth angles above 270° or below 90°. Histograms for each incidence angle range are evaluated for each study region for adequate azimuthal diversity. Incidence angle ranges of $\pm 2.5°$ and $\pm 1.5°$ are examined for each study region over the incidence angles from 25° to 55°. Ranges of $\pm 1.5°$ around the average incidence angle of 40° provide good azimuth angle diversity with an acceptably narrow range of incidence angles.

A total of 14 study regions near the edge of the sea ice pack are selected to study azimuthal modulation in the MIZ during the winter freeze up. The penetration of long wavelength swell waves into the uncoalesced MIZ sea ice may result in enough surface slope to induce azimuthal modulation not coupled to sea ice surface characteristics. The MIZ study regions are selected based on enhanced-resolution imagery and are selected to include regions where wave penetration is likely. Note in Fig. 3 the bright area near the ice pack edge. The subresolution scatterers in the MIZ cause a brighter microwave signature than other parts of the sea ice pack and have been observed in the Labrador Sea MIZ [8].

Although the manual evaluations provide only a crude consistency check of the data, the check is sufficient for reviewing time periods and parameter ranges suitable for evaluating azimuthal modulation. A total of 19 study regions in the Antarctic sea ice pack at various times of the year

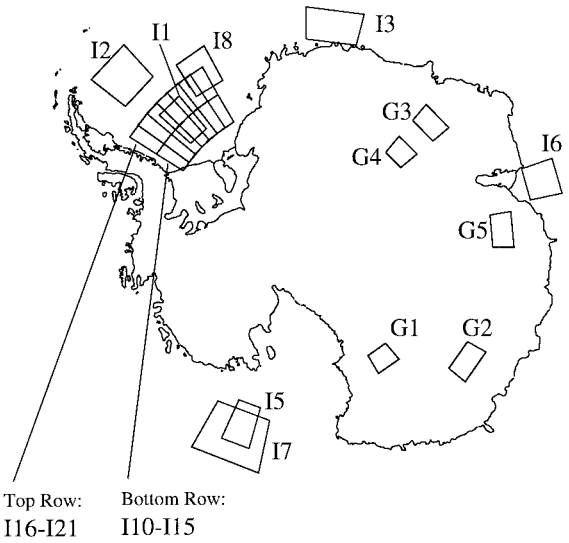

Fig. 5. Study regions used with the ERS-1 data. The boxes indicate the location of the data. Different time periods are used for the various boxes. All data is from 1993. Regions I10 through I21 are overlapping regions in the Weddell sea.

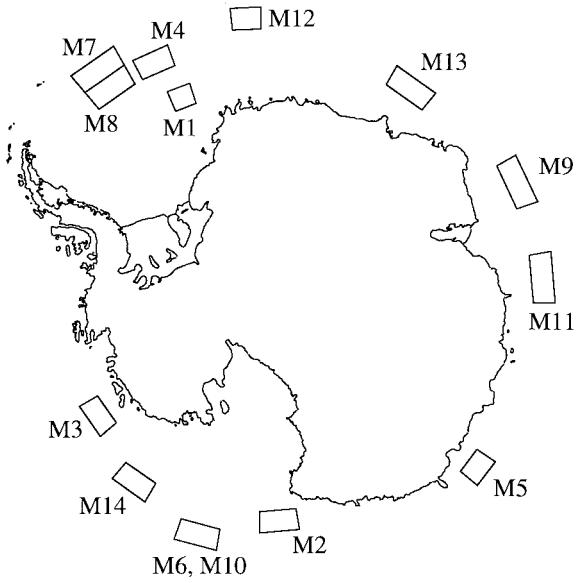

Fig. 6. MIZ study regions used with the ERS-1 data. The boxes indicate the location of the data. Different time periods are used for the various boxes. All data is from 1993. These regions were selected to be near the sea ice pack edge.

in 1993 are selected and used in this study, as well as 14 additional regions selected near the ice edge. The study regions are illustrated in Fig. 5, and statistics for each region are given in Table I. The 14 MIZ areas are illustrated in Fig. 6, with statistics in Table II. The study regions in the Weddell Sea are large and overlapping to provide a better picture of the characteristics of the sea ice pack in this highly dynamic region. The julian day (JD) in Tables I and II reflect the time period for which data was extracted in each region. In practice, smaller day ranges are used in evaluating azimuthal modulation to better approximate constant surface conditions.

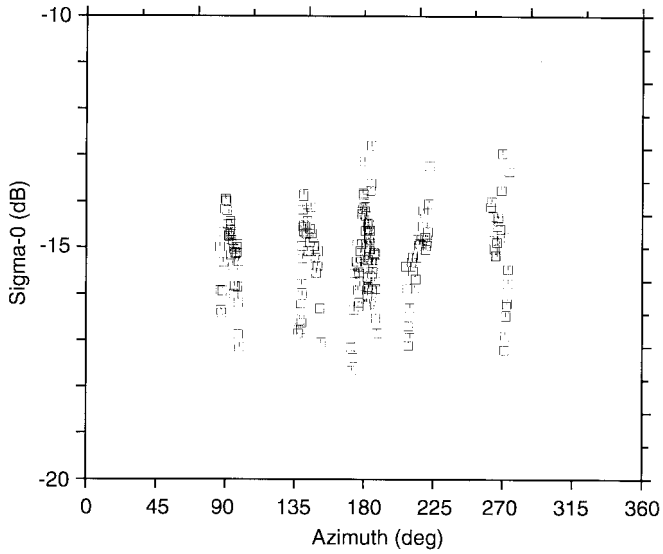

Fig. 7. Representative σ^o versus azimuth angle plot for sea ice. This region is in the Weddell Sea region I1 in Fig. 5. $\hat{\mathcal{A}}$, which is the incidence angle normalized σ^o, is plotted.

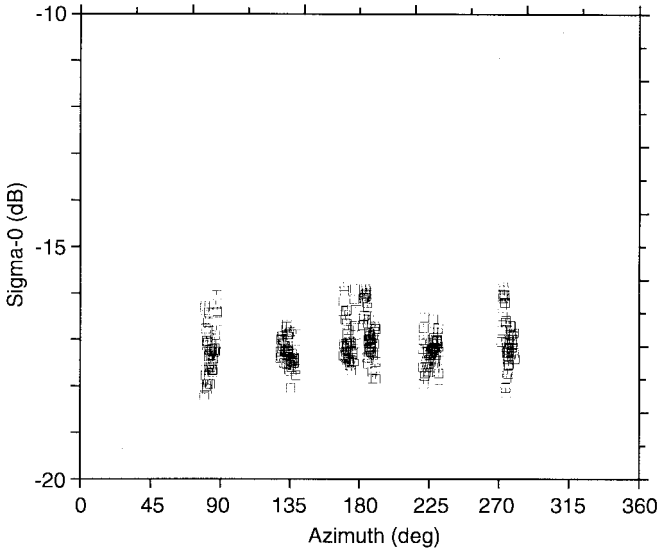

Fig. 8. Representative σ^o versus azimuth angle plot for sea ice. This region is in the Weddell Sea region I8 in Fig. 5. $\hat{\mathcal{A}}$, which is the incidence angle normalized σ^o, is plotted.

IV. Analysis

The data is analyzed using two different methods. First, by assuming that the data in each study region is representative of a single type of sea ice, the diversity of azimuth angles in each study region data set leads to a natural test for azimuthal modulation: plotting $\hat{\mathcal{A}}$ versus azimuth angle. If the σ^o spread in the data is low, any azimuthal modulation should be apparent in these plots. Using small incidence angle ranges reduces error introduced by the necessary correction for incidence angle dependence.

Second, the fore-aft beam difference is examined. Because the fore and aft beams are 90° apart in azimuth, any significant difference in azimuth response is likely to appear as a difference between the fore and aft beam measurements. In addition, because the fore and aft beams have identical incidence angles, no correction for incidence angle dependence is necessary, thus eliminating a potential source of error in the analysis.

A. $\hat{\mathcal{A}}$ versus Azimuth

Figs. 7 and 8 show representative plots of $\hat{\mathcal{A}}$ versus azimuth angle for small incidence angle ranges (37–39°) over sea ice. For comparison, Fig. 9 shows a representative plot of $\hat{\mathcal{A}}$ versus azimuth angle for a small incidence angle range over the Antarctic ice sheet. The range of $\hat{\mathcal{A}}$ is relatively high in the ice sheet regions but is comparable to the spread found in plots of ice sheet response in Remy *et al*. [7]. These plots are representative of the graphs produced in this study for all land and sea ice regions.

Based on the discussion in Section III-B, we can ignore incidence angle dependence when the data is taken over a 3–4° range. A comparison of corrected and uncorrected plots over small incidence angle ranges shows little difference if the normalization angle is chosen to be within the incidence angle range.

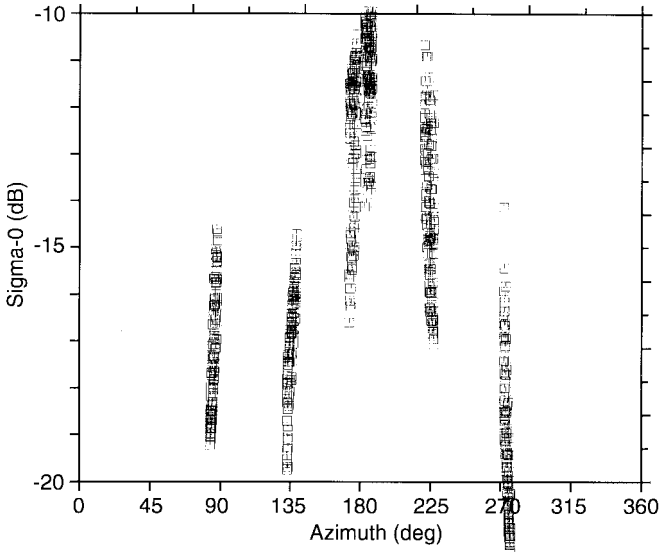

Fig. 9. Representative σ^o versus azimuth angle plot for Antarctic glacial ice. $\hat{\mathcal{A}}$, which is the incidence angle normalized σ^o, is plotted.

An examination of Figs. 7 and 8 shows negligible azimuth angle modulation over sea ice. In all sea ice regions studied, the observed variation in azimuth angle of σ^o was less than 1 dB. Note that the plot in Fig. 9 shows significant modulation in azimuth in microwave signatures over land ice sheets.

B. Fore-Aft Pair Analysis

Because the fore and aft beams have nearly identical incidence angles and azimuth angles 90° apart, it is probable that azimuthal modulation will be displayed in the difference between the fore and aft beam measurements. In this analysis, the simple difference between fore and aft beam measurement pairs are calculated, and bulk statistics for each study region

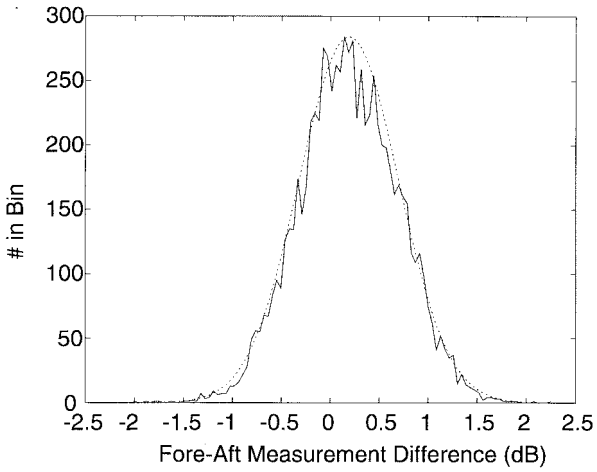

Fig. 10. Histogram of the difference of the fore and aft beams from the raw scatterometer data for region I10. The dotted line is a Gaussian curve based on the mean and standard deviation of the actual histogram.

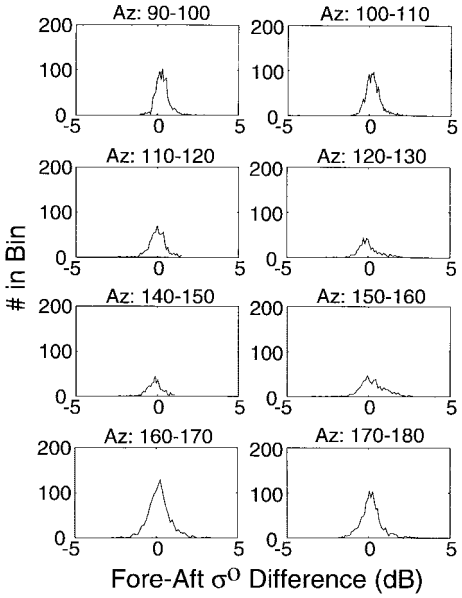

Fig. 11. Histogram of the difference of the fore and aft beams from the sea ice region I12. These graphs are over small azimuth angle ranges as noted over each graph and illustrate the stability of the histogram mean in azimuth. If the data set does not have measurements in an azimuth range, that azimuth range is not illustrated in the figure.

are examined. In addition, the fore–aft difference over a limited azimuth range is examined over sea ice and land ice.

The difference between the fore and aft beam measurements may be modeled by

$$D = (\sigma_F^o + N_F) - (\sigma_A^o + N_A) \tag{6}$$

where N_F and N_A are independent Gaussian noise terms associated with the fore and aft beam measurements, respectively. We can predict D over an azimuthally isotropic medium. For an azimuthally isotropic medium, $\sigma_F^o - \sigma_A^o = 0$ since the incidence angles for each measurement are equal, and D becomes the difference of the noise terms:

$$D = N_F - N_A. \tag{7}$$

Since the sum of two independent Gaussian random variables is a Gaussian random variable, we expect the fore–aft beam measurement difference to be a Gaussian random variable. Assuming the noise terms are zero mean, a histogram of fore–aft beam measurement differences will be a zero mean Gaussian distribution if the observed surface is isotropic in azimuth.

Fig. 10 shows an example histogram of the sea ice regions studied. The histogram is over all available azimuth angles. The dotted Gaussian curve fitted to the example sea ice azimuth angle histogram is based on the mean and standard deviation of the data in the histogram. As predicted, the data is Gaussian with a nearly zero mean. For all the regions studied, the mean is less than 0.2 dB in every case. Fig. 11 shows similar histograms for the same region but over 10° azimuth angle ranges. Note that the mean remains constant in each azimuth angle bin, which is not the case over land ice [6], as illustrated in Fig. 12, which shows a histogram from a land ice region. Over the bulk of the data in this land ice region, there is a nonzero difference between the fore and aft beams, suggesting that there is modulation in the ice sheet microwave signature. Fig. 13 shows the same data but with histograms over 10° incidence angle ranges (compare with Fig. 11). Note the

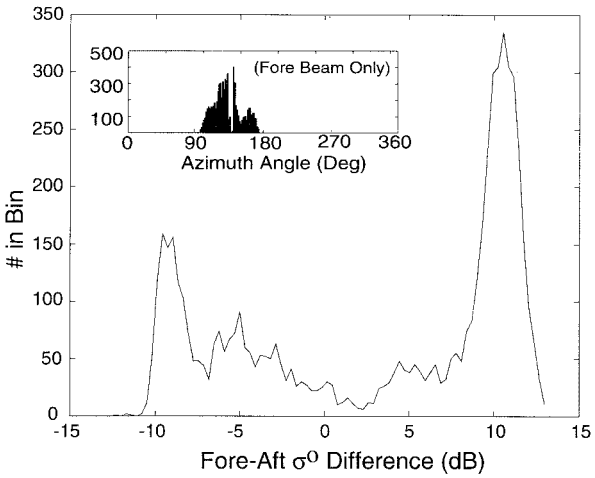

Fig. 12. Histogram of the difference of the fore and aft beams for scatterometer data from glacial region G2. The inset is a histogram of azimuth angles from the fore beam only to illustrate the diversity of azimuth angles in this study region.

progression of mean from positive at lower azimuth to negative at higher azimuth. A plot of the mean fore–aft difference for 5° azimuth bins versus azimuth angle is shown in Fig. 14. The double sinusoid plot is similar to the Ku-band results of Remy *et al.* [7] and is very similar to the geophysical model function used for retrieving near surface ocean winds illustrated in [21].

C. Marginal Ice Zone

Of special concern are regions of sea ice near the periphery of the sea ice pack. Unlike areas of open ocean, we do not expect gravity or capillary waves to form and create azimuthal

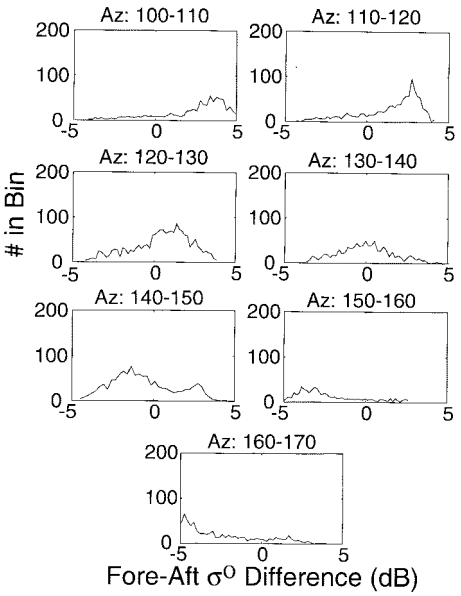

Fig. 13. Histogram of the difference of the fore and aft beams for scatterometer data from glacial region G2 over 10° azimuth ranges from 80–180° (fore beam only). Note the progression of the mean from positive to negative as azimuth increases.

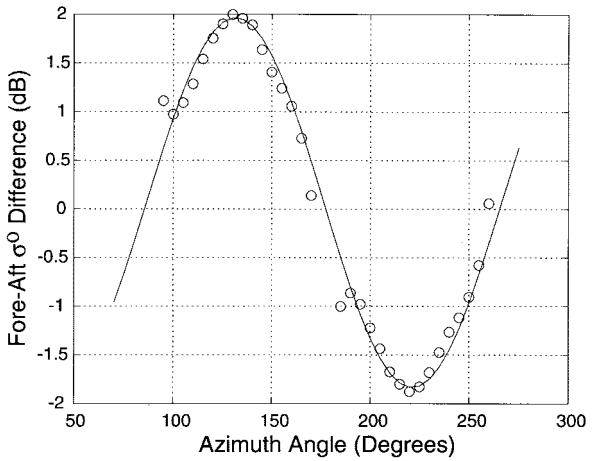

Fig. 14. Example histogram of azimuthal angles over Antarctic sea ice (Study Region I10). Note that the gaps are caused by the instrument geometry. Line is theleast-squares fit to $\cos 2_x$.

modulation in the microwave signature. However, because long wavelength swell waves can propagate deep into the sea ice pack, a surface slope may be created that is sufficient to induce azimuthal modulation in σ^o. However, given that these swell waves can have wavelengths on the order of several kilometers or more and amplitudes on the order of a few meters, the change in surface slope is quite small. Fourteen regions near the edge of the sea ice pack were selected between JD 102 and JD 204 1993 and reviewed for azimuthal modulation using a fore–aft difference analysis. Using the previously described methodology, it is determined that azimuth modulation in all regions studied was less than 1 dB. Further, in the majority (11 of 14), the azimuth modulation is less than 0.2 dB. We conclude that on the scale of the scatterometer measurements, no azimuthal modulation is visible over Antarctic sea ice.

V. Summary

A detailed analysis of C-band ERS-1 scatterometer data reveals that there is no significant azimuthal modulation (less than 1 dB) evident in data taken over Antarctic sea ice at the scale of the ERS-1 scatterometer measurements (nominally 50 km). Similar results have been recently obtained for Ku-band NSCAT data. The consistency of the analysis methods used in this study was established by comparing sea ice results with land ice sheet results. Using the same methodologies for both land and sea ice, azimuthal modulation is shown to be negligible in the sea ice regions studied. In contrast, land ice study regions exhibit significant azimuthal modulation. This result is consistent with the results of previous studies of azimuthal modulation over land ice sheets. Areas in the MIZ, where long wavelength swell waves can penetrate deep into the ice pack, also displayed negligible levels of azimuthal modulation in the ERS-1 scatterometer measurements.

Acknowledgment

The authors would like to thank Dr. R. Thomas and Dr. G. Assrar at NASA for their support of this research, ESA for the use and availability of the ERS-1 scatterometer data, and Dr. M. Drinkwater and the reviewers for their insightful comments and suggestions regarding this manuscript.

References

[1] D. G. Long and P. J. Hardin, "Vegetation studies of the amazon basin using enhanced resolution seasat scatterometer data," *IEEE Trans. Geosci. Remote Sensing,* vol. 32, pp. 449–460, 1994.

[2] D. Long and M. Drinkwater, "Greenland ice-sheet surface properties observed by the seasat—A scatterometer at enhanced resolution," *J. Glaciology,* vol. 40, no. 135, pp. 213–230, 1994.

[3] M. Drinkwater, D. Long, and D. Early, "Enhanced resolution ERS-1 scatterometer imaging of Southern Ocean sea ice," *ESA J.*, vol. 17, pp. 307–322, 1993.

[4] A. R. Hosseinmostafa *et al.*, "Comparison of radar backscatter from Antarctic and Arctic sea ice," *J. Electromag. Waves Appl.,* vol. 9, no. 3, pp. 421–438, 1995.

[5] P. Lecomte, A. Cavanie, and F. Gohin, "Recognition of sea ice zones using ERS-1 scatterometer data," in *Proc. IGARSS*, 1993, pp. 855–857.

[6] D. Long, P. Hardin, and P. Whiting, "Resolution enhancement of spaceborne scatterometer data," *IEEE Trans. Geosci. Remote Sensing,* vol. 31, pp. 700–715, 1993.

[7] F. Remy, A. Ledroit, and J. F. Minster, "Katabatic wind intensity and direction over Antarctica derived from scatterometer data," *Geophys. Res. Lett.,* vol. 19, pp. 1021–1024, 1992.

[8] C. E. Livingstone and M. R. Drinkwater, "Springtime C-band SAR backscatter signatures of Labrador Sea marginal ice: Measurements versus modeling predictions," *IEEE Trans. Geosci. Remote Sensing,* vol. 29, pp. 29–41, Jan. 1991.

[9] E. Attema, "The active microwave instrument onboard the ers-1 satellite," *Proc. IEEE,* vol. 79, pp. 791–799, 1991.

[10] M. R. Drinkwater, R. Hosseinmostafa, and W. Dierking, "C-band microwave backscatter of sea ice in the Weddell Sea during the winter of 1992," in *Proc. IGARSS*, 1993, pp. 446–448.

[11] J. Comiso *et al.*, "Microwave remote sensing of the Southern Ocean ice cover," in *Microwave Remote Sensing of Sea Ice,* F. D. Carsey, Ed. Boston: Amer. Geophys. Union, 1992, ch. 12.

[12] M. A. Lange, S. F. Ackley, P. Wadhams, G. S. Diekmann, and H. Eicken, "Development of sea ice in the Weddell Sea," *Ann. Glaciology,* no. 12, pp. 92–96, 1991.

[13] M. R. Drinkwater and C. Haas, "Snow, sea ice, and radar observations during ANT X/4: Summary data report," Alfred Wegener Inst., Tech. Rep. 53, July 1994.

[14] P. Gloersen *et al.*, *Arctic and Antarctic Sea Ice, 1978–1987: Satellite Passive-Microwave Observations and Analysis.* Washington, DC: NASA, 1992.

[15] V. I. Lytle and S. F. Ackley, "Sea ice ridging in the eastern Weddell Sea," *J. Geophys. Res.,* vol. 96, no. 10, pp. 18411–18416, 1991.
[16] W. Dierking, "Laser profiling of the ice surface topography during the winter Weddell gyre study 1992," *J. Geophys. Res.,* vol. 100, no. C3, pp. 4807–4820, 1995.
[17] A. K. Liu and S. Häkkinen, "Wave effects on ocean-ice interaction in the marginal ice zone," *J. Geophys. Res.,* vol. 98, no. C6, pp. 10025–10036, 1993.
[18] M. Drinkwater, D. Early, and D. Long, "ERS-1 investigations of Southern Ocean sea ice geophysics using combined scatterometer and SAR images," in *Proc. IGARSS*, 1994, pp. 165–167.
[19] M. Pettersson *et al.*, "Analysis of C-band backscatter measurements of thin Arctic sea ice," in *Proc. IGARSS*, 1995, pp. 360–362.
[20] D. Long, D. Early, and M. Drinkwater, "Enhanced resolution ERS-1 scatterometer imaging of southern hemisphere polar ice," in *Proc. IGARSS*, 1994, pp. 156–158.
[21] M. H. Freilich and R. S. Dunbar, "A preliminary C-band scatterometer model function for the ERS-1 AMI instrument," in *Proc. First ERS-1 Symp.,* Cannes, France, 1993, ESA, pp. 79–84.
[22] M. Drinkwater, personal communication.

David S. Early (S'93) received the B.S. degree in electrical engineering from Brigham Young University (BYU), Provo, UT, in April 1993. He is currently a Ph.D. candidate at BYU.

He has worked with the Microwave Earth Remote Sensing Group at BYU since 1992. Current research interests center on resolution enhancement techniques for satellite radar systems, specifically the theory behind such techniques and the scientific application of resolution-enhanced scatterometer data.

Mr. Early received a 1993 NASA Global Change Fellowship.

David G. Long (M'89) received the B.S. and M.S. degrees in electrical engineering from Brigham Young University (BYU), Provo, UT, in 1982 and 1983, respectively, and the Ph.D. degree in electrical engineering from the University of Southern California, Los Angeles, in 1989.

He worked for the Jet Propulsion Laboratory (JPL), California Institute of Technology, Pasadena, as a radar systems engineer from 1983 through 1990. He served as the Project Engineer for the NASA Scatterometer (NSCAT) project and as the Experiment Manager for the EoS SCANSCAT (now SeaWinds) project. He was also a group leader supervising a staff of system engineers working on a number of JPL flight projects. While at JPL, he was responsible for the high-level design and system performance analysis of NSCAT. He is now an Associate Professor in the Electrical and Computer Engineering Department at BYU, doing research in microwave remote sensing and mesoscale atmospheric dynamics. He is a member of the NSCAT Science Working Team. His research interests include signal processing, estimation theory, radar, air/sea interaction, and mesoscale atmospheric dynamics.

Dr. Long has received the NASA *Certificate of Achievement* several times. He is a member of AGU, Sigma Xi, and Tau Beta Pi.